514

Physica Scripta. Vol. 38, 291–296, 1988.

Spin-Polarized Electron Microscopy

Daniel T. Pierce

National Bureau of Standards, Gaithersburg, MD 20899, U.S.A.

Received November 18, 1987; accepted November 24, 1987

Abstract

A current scientific challenge with many ramifications for magnetic technology is to image magnetic microstructure with the highest possible spatial resolution in order to observe magnetic domains or even spin configurations within a domain wall. Ultimately one can envision imaging the magnetic moment of individual atoms which would also make possible the observation of antiferromagnetic structures. The measurement of the spin polarization of secondary electrons generated by a finely focussed (unpolarized) scanning electron microscope (SEM) beam to obtain high-resolution magnetization images is presented. An alternative measurement, using a spin-polarized incident beam in an SEM, has many difficulties which are discussed. To measure spin configurations with higher spatial resolution, the possibility of introducing electron spin polarization in scanning field-emission and tunneling microscopy is considered. The measurement of the spin polarization of secondary electrons generated by a specially prepared single-atom scanning field-emission tip looks promising. High-resolution imaging of spin configurations in scanning tunneling microscopy appears possible if the tip itself is a source of spin-polarized electrons. The potential advantages and unsolved problems involved in using a ferromagnetic tip or an optically pumped semiconductor tip are described.

1. Introduction

The aim of spin polarized electron microscopy is to reveal electron spin configurations. At a spatial resolution of order 1000 Å, the polarized electron microscopy might image the shape of the magnetic domains of a ferromagnet. A ferromagnet breaks up into domains to minimize its free energy which consists of several contributions, among them the exchange energy, the crystalline anisotropy energy, and the magnetostatic energy. Domain configurations can be calculated only in the most ideal cases. In general, they are very complex and can be determined only by observation. Domain configurations are not only of fundamental interest, but are also of great technical importance. The domain size and sharpness of its boundary are factors limiting the increase in density and the reduction of noise in magnetic storage. At somewhat higher resolution of order 100 Å, polarized electron microscopy might be used to determine the spin configuration across a domain wall, i.e., the boundary between domains. For thin (< 500 Å) films, the walls are of the Nèel type and the spins rotate in the plane of the film in going from one domain to the next whereas in thicker films (> 1000 Å) the spins rotate in a plane normal to the surface producing a Bloch wall. At intermediate thicknesses, complex cross-tie walls are observed. The details of such spin configurations remain to be investigated. At extremely high resolution of a few Å, one can imagine imaging atomic spin configurations. With sufficient resolution one could observe the alternating spins in an antiferromagnet or the spin vortex structure postulated in the x–y model of a 2-dimensional ferromagnet.

Most present methods for investigating spin configurations are indirect and reflect the effect of the magnetic field due to a net spin density. For example, in the Bitter method [1] fine magnetic particles are collected in the stray magnetic fields at domain walls. In Lorentz microscopy, the probing electrons are deflected by the magnetic field in the sample. In an electron microscope, rather limited resolution is achieved by Lorentz microscopy in the reflection mode (~ 1 μm) [2] although quite high resolution (~ 10 nm) can be achieved in the transmission mode [3] at the expense of thinning the sample to of order 1000 Å which may in turn affect its magnetic properties. The magneto-optic Kerr effect [4] is a direct method in that the Kerr rotation is directly proportional to the magnetization, i.e., the magnetic moment or spin density per unit volume. The spatial resolution of the Kerr effect, an optical technique, is typically ~ 1 μm.

In this paper we consider how spin configurations can be directly probed with spin polarized electron techniques. We first discuss Scanning Electron Microscopy with Polarization Analysis (SEMPA), the recently developed technique in which one measures the spin polarization of secondary electrons emitted from a ferromagnetic sample when hit by an unpolarized incident beam in a SEM [5, 6]. Domain images have been successfully obtained from a variety of materials including an Fe–3% Si single crystal, a permalloy thin film recording head, a CoNi recording material, and an amorphous ferromagnet. We then discuss the potential advantages and disadvantages of an alternative technique in which the incident electron beam in an SEM is itself spin polarized and one measures variations in the current absorbed by, or intensity of electrons scattered from, the ferromagnetic target. These two ways of combining spin polarized electrons and the SEM form the context in which we can consider ways to extend the limits of resolution to achieve the ultimate goal of atomic resolution. We discuss two paths toward atomic resolution which take advantage of recent experience gained with scanning tunneling microscopy (STM). In the first, the spin of secondary electrons generated by a scanning field-emitter tip is measured. In the second, spin-polarized electron tunneling, wherein the tip is a source of spin polarized electrons, is described.

2. Scanning electron microscopy with polarization analysis (SEMPA)

The principle of SEMPA is illustrated in Fig. 1. A focused electron beam is scanned across the specimen causing secondary electrons to be emitted. The magnitude and direction of the spin polarization of the secondary electrons emitted from a ferromagnet is directly proportional to the magnitude and direction of the magnetization in the region probed by the incident electron beam. By measuring the secondary electron polarization as the incident beam is rastered across the speciman, one obtains an image of the magnetization. The nature

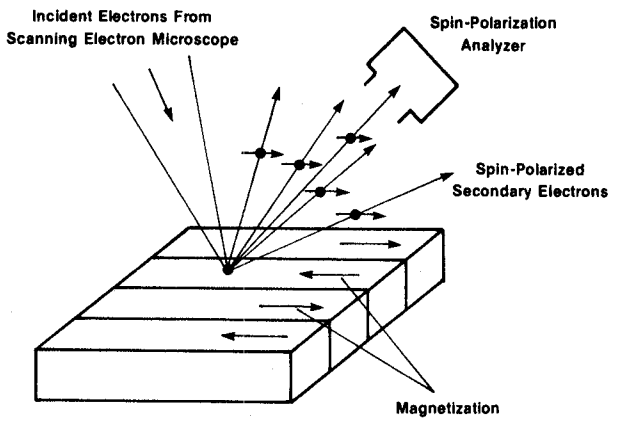

Fig. 1. Principle of scanning electron microscopy with polarization analysis (SEMPA).

of the measurement is such that magnetization images can be obtained from a thick magnetic specimen or from a magnetic structure on a non-magnetic substrate, such as a permalloy memory element on a silicon chip.

The spin polarization along, for example, the z direction is

$$P_z = \frac{N\uparrow - N\downarrow}{N\uparrow + N\downarrow} \tag{1}$$

where $N\uparrow(N\downarrow)$ is the number of electrons with spins parallel (antiparallel) to the z direction. The peak at low energy in the energy distribution of secondary electrons, which is due largely to the excitation and decay of electron–hole pairs, is both large and highly spin polarized [7]. A uniform excitation of valence electrons in a ferromagnetic specimen would give for the polarization

$$P = n_B/n. \tag{2}$$

Here n is the average number of valence electrons per atom and $n_B = n_\uparrow - n_\downarrow$ is the net spin density per atom, also known as the Bohr magneton number. The polarization values expected from eq. (2) for Fe, Co, and Ni are 0.28, 0.19, and 0.05 respectively. This high degree of spin polarization provides excellent contrast and the large number of secondary electrons provides a large signal. The quantity $(N\uparrow + N\downarrow)$ in eq. (1) is the usual secondary electron signal which can be used to obtain an image of specimen topography. This signal is measured simultaneously but independently of P so that the magnetic image is independent of the topographic image.

The spatial resolution of SEMPA is determined by the size of the electron beam in the SEM and by electron scattering in the specimen [2]. The specimen must be at a distance of approximately 1 cm from the objective lens pole piece in order to extract secondary electrons and minimize disturbing magnetic fields from the objective lens. Thus, in SEMPA it may not be possible to achieve the ultimate resolution of an SEM specified at a shorter working distance.

The measurement of spin polarization relies on the spin–orbit interaction in the scattering of a polarized electron beam from a heavy-element target such as gold. It is an inefficient process, and many more electrons must be counted to obtain a polarization image than a topographic image. The statistical uncertainity ΔP in the measurement of the polarization of beams of N electrons is [8]

$$\Delta P = \sqrt{\frac{1}{FN}} \tag{3}$$

where F is the figure of merit of a spin analyzer and even for the best analyzer is of order 10^{-4} [9]. Even though the secondary electron signal is large, the time for a magnetization image is of order 10 minutes owing to the spin analysis. The time required for a measurement and the positional stability of the SEM, along with the limitations on the current available within a given beam diameter, all limit the ultimate resolution of SEMPA, but a resolution of ~ 50 nm has been achieved and a resolution < 10 nm appears practical. New compact spin analyzers have been developed [9] for SEMPA, although traditional Mott analyzers were used in the first experiments [10].

An example of a SEMPA magnetic image is shown in Fig. 2(a). An image of the magnetization along an orthogonal direction is obtained simultaneously with the intensity image showing the topography which is displayed in Fig. 2(b). In this Fe–3% Si specimen, the three defects observed in the topographic image of Fig. 2(b) appear to pin the domain walls of the magnetization image. The component of the magnetization along the measurement axis is indicated by the gray levels of the magnetization image. The excellent performance of SEMPA in imaging domain configurations has been demonstrated on a wide variety of materials.

3. Electron microscopy with a polarized incident beam

Given the inefficiency of currently available spin polarization analyzers, it is natural to consider [11, 12] alternative

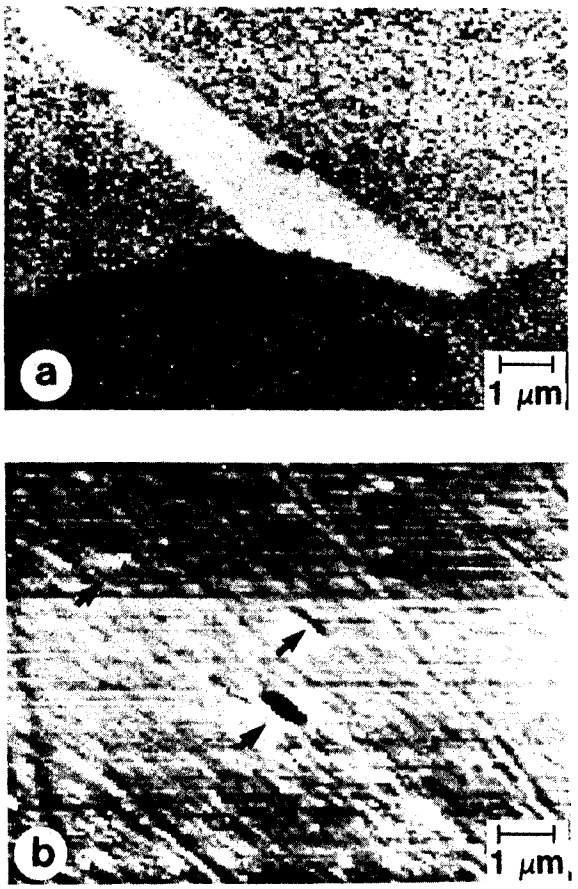

Fig. 2. A SEMPA image of (a) one component of the electron spin polarization and (b) of the intensity from a Fe–3% Si crystal. Three different magnetization regions (three different directions of spin orientation) are depicted by the three different gray levels in (a). The dagger shaped domain appears to have its walls pinned by the defects evident in the topographic image (b).

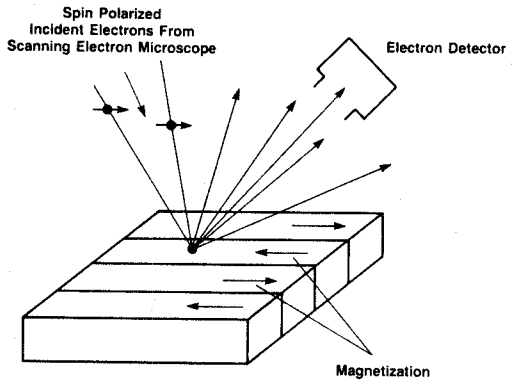

Fig. 3. Principle of spin polarized scanning electron microscopy using a spin polarized beam is the SEM column and detecting the differences in scattered intensities depending on orientation of spins in the magnetic target. Only the intensity, not the spin polarization, of the scattered electrons need be measured.

approaches to spin polarized microscopy where this inefficiency can be avoided. It was demonstrated several years ago that, when a spin polarized electron beam is scattered from a ferromagnetic surface, there is a difference in the scattered intensity for incident electron spin polarization parallel and antiparallel to the magnetization [13]. Subsequent measurements showed that there is a related asymmetry in the number of electrons absorbed by the target [14]. A polarized electron microscopy that takes advantage of these effects is shown in Fig. 3. In contrast to Fig. 1, no spin analyzer is required which increases the efficiency by approximately 10^4.

The spin-dependent scattering asymmetry is defined as

$$A = (I\uparrow - I\downarrow)/(I\uparrow + I\downarrow) \tag{4}$$

where $I\uparrow$ ($I\downarrow$) is the scattered intensity for incident-beam electron spin polarization parallel (antiparallel) to the net spin density of the ferromagnetic sample. Typical intensity asymmetries are only a few percent and one usually detects the intensity asymmetry synchronously with the periodic reversal of the spin polarization of the electron beam. An intense beam of electrons with up to 50% spin polarization is obtained by photoemission of electrons which are excited in GaAs by circularly polarized light [15]. The electron spin polarization is reversed by changing from right to left circularly polarized light. The GaAs surface is treated with cesium and oxygen to lower the vacuum level such that very high quantum yields are obtained. However, a GaAs photocathode has not been used in an electron microscope, and the ultimate limitations on the brightness of such a cathode have not been tested. Certainly a very bright cathode emitting polarized electrons can be obtained using a EuS coated W field emission tip; however, the polarization is not easily reversed and the tip must be operated at 10 K [16].

Although this type of polarized electron microscopy would have the advantage that only an intensity measurement is required, there are a number of disadvantages. The spin dependent scattering asymmetry is largest for incident electrons with an energy of about 100 eV and decreases steadily for higher electron beam energies [17]. Operating an SEM at an energy $\langle 200$ eV severely limits the resolution to 50–100 nm in the best microscopes. One must also worry about the depolarization of the electron beam in the magnetic fields of the SEM lenses. Finally, spin-independent factors such as sample roughness or crystallite structure can affect the asymmetry, and hence the magnetic image, because the asymmetry depends on the angle of the incident beam with respect to crystal planes. Clearly there are many problems with polarized electron microscopy using a spin-polarized incident beam. As a consequence, to date it has been contemplated but not tried. It does, however, provide a useful conceptual analogy for considering the possibility of obtaining very high resolution with polarized scanning tunneling microscopy.

4. Scanning field emission/tunneling microscopy with polarization analysis

The highest resolution images of surface topography on an atomic scale have been obtained with the scanning tunneling microscope (STM) [18]. The ultimate goal of polarized microscopy is to image spin configurations with atomic resultion also. As a first means of making a STM sensitive to spin configurations, consider the analogy to SEMPA. It is envisioned that incident electrons from a scanning tip would generate secondary electrons which would be extracted for spin polarization analysis. In the STM mode where the tip to sample bias is < 1 V and the spacing is a few Å, a SEMPA-like measurement is not realistic. Rather we consider the scanning field emission mode with a few tens of volts bias voltage and several tens of Å spacing. The questions are: (1) can secondary electrons be observed in sufficient number; and (2) what spatial resolution can be obtained?

Secondary electrons were observed many years ago in an STM-like instrument operated in the scanning field emission mode at a bias voltage of 160 V and a spacing of order 1000 Å [19]. More recently, the energy distribution of the secondary electrons generated in the scanning field-emission mode (tip to sample voltage ~ 1 keV and spacing ~ 1 mm) has been measured and peaks due to Auger transitions have been identified [20]. The lateral spatial resolution in each of these examples of scanning field emission microscopy was of order 1 μm and therefore not yet attractive when compared to SEMPA (Section 2).

What are the limits of resolution in the scanning field emission mode? Fink has made single-atom tips [21] and used these to generate secondary-electron topographic images which suggest that a lateral resolution of 30 Å or better may be achieved in the scanning field-emission mode at a bias voltage of 15 V and spacing of a few nm [22]. The secondary electron count rates at a nearby electron multiplier exceeded 10^5 s and could be higher with improved extraction electron optics. The angular spread (full cone angle) of the beam from single-atom tips was reported to be 3–4° for an electron beam and 1° for an ion beam when atoms in a background gas are field-ionized at such a tip [22]. Both electrons and ions generate secondary electrons that can be used for secondary-electron imaging. Just what secondary electron intensity can be obtained at a specified spatial resolution, and whether the secondaries can be extracted without scattering between specimen and tip, are questions which require further investigation. However, scanning microscopy in the field emission mode with single atom tips looks very promising as a means to achieve high resolution in polarized electron microscopy.

5. Scanning spin-polarized tunneling microscopy

In this section we consider the scanning tunneling analog to

electron microscopy with a polarized incident beam that was discussed in Section 3. The sample contains the spin configuration to be probed and the tip provides a tunneling current of spin-polarized electrons. The tunneling conductance will depend on the electron spin configuration of the sample and the overlap of these states with the polarized electron states of the tip. We discuss two ways in which a tip could be a source of polarized electrons, namely (1) a ferromagnetic tip or (2) an optically pumped semiconductor tip.

5.1. *Tunneling from a ferromagnetic tip*

Measurements of the spin polarization of field-emitted electrons offer a guide to promising sources of polarized electrons for microscopy. Polarization values from Fe have been measured to be 25% for tips oriented along the [100] axis and 20% for tips oriented along the [111] axis [23]. This is a substantial degree of polarization, especially since nearly unpolarized *s*, *p* electrons are generally believed to tunnel with 10 to 100 times the probability of the *d* states [24].

Another possibility is the EuS-coated W tip [16] already mentioned in Section 3. Here the polarization mechanism is different. The EuS acts as a filter for electrons from W. Those electrons that go into the higher lying spin-split band of the EuS have a much higher probability of tunneling through the field emission barrier, giving $P \simeq 90\%$ at 10 K [16]. The Curie temperature of EuS is 16 K.

One would like to know the orientation of the electron spins at the tip and ideally, to control this orientation. The strong shape anisotropy of an iron field-emission tip leads to the expectation that the electron spin polarization is along the tip axis. The direction could be reversed by application of an appropriate magnetic field, for example, by pulsing a small coil around the tip. The spin orientation of electrons from a W/EuS tip can be along the tip axis or transverse to it depending on tip preparation [16]. For any ferromagnetic tip, one must worry about the effect of the magnetic field of the sample on the tip and of the tip on the sample which may be large at tunneling distances.

One of the problems of a polarized STM measurement will be to separate the spin-dependent signal from the signal due mainly to the topography. One straightforward way to separate these signals is to modulate the direction of spin polarization of the tunneling electrons by reversing the magnetization direction in the tip. It has not yet been demonstrated that this can be readily done with the ferromagnetic tips discussed. An alternative way to emphasize the spin-dependent signal is illustrated in Fig. 4. Consider a ferromagnetic sample with domains with magnetization either out of or into the surface, that is, along the presumed polarization direction of an Fe tip. For the sake of discussion, let the sample have filled majority-spin *d* bands. The bias is varied between two values, V_1 as in Fig. 4(a) where the tunneling is primarily into *s*, *p* like states, and V_2 as in Fig. 4(b) where the tunneling is into predominantly d states. As depicted in Fig. 4(c), the tunneling current is larger when the domain orientation is such that the minority-spin holes are oriented like the polarized tunneling electrons and there will be no tunneling into *d* states when the domain magnetization is oppositely oriented. The tunneling at V_1 into the *s*, *p* states is expected to be the same regardless of magnetization direction in a domain. As the tip is scanned, the change in the ratio of tunneling at V_2 to that at V_1 gives the magnetic signal and is

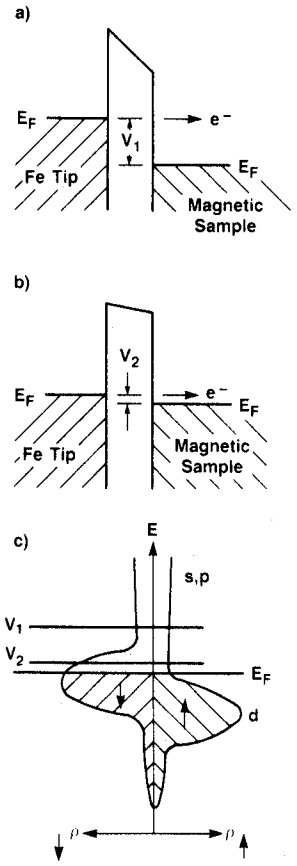

Fig. 4. Schematic of tunneling from a ferromagnetic tip into a ferromagnetic sample. In (a) the negative tip bias V_1 relative to the sample is greater than the bias V_2 in (b). Illustration (c) of how the bias V_1 of (a) emphasizes tunneling into *s*, *p* states and bias V_2 of (b) allows tunneling into highly polarized *d* states.

insensitive to the effect of changing topography. The "gated" mode of STM operation is used to assure that the tunneling distance does not vary during the scan.

It is envisioned that this experiment will be in ultrahigh vacuum and that the tip and sample will be free of contaminants. It is our experience that adsorbates on a ferromagnetic surface can drastically alter the surface magnetic properties. In previous conventional tunneling experiments between ferromagnetic films separated by a barrier layer, only very small magnetic effects were observed and then only at $T = 4.2$ K [25]. It is, in principle, possible to do STM through the energy gap of an oxide on a ferromagnetic surface. This may allow experiments in air rather than in UHV for benign oxides or other insulating overlayers which are sufficiently thin.

5.2. *Tunneling from an optically pumped semiconductor*

In this section we consider optically pumping a semiconductor to achieve a tip from which the tunneling current is spin polarized. Optically-pumped negative electron affinity GaAs is widely used as a source of polarized electrons in many spin-polarized electron studies. When GaAs is used as a photocathode in an electron gun, the vacuum level is lowered with cesium and oxygen to allow the escape of conduction band electrons into vacuum. However, for tunneling between GaAs and a magnetic sample shown schematically in Fig. 5, no surface treatment of the GaAs is required, and the tunneling takes place through the approximately rectangular barrier shown. In contrast to photo-assisted field emission

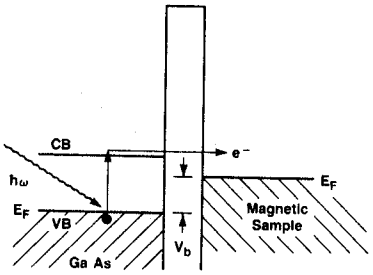

Fig. 5. Schematic diagram showing the photoexcitation (via circularly polarized light) of spin polarized electrons to the conduction band of GaAs. The electrons then tunnel into the magnetic sample where different states can be probed by varying the bias voltage V_b as in the preceding figure.

[26], in which photo-excited electrons see a much narrower part of a triangular barrier and emission is greatly enhanced, photo-excited electrons in GaAs experience only small gains in tunneling probability.

The significant advantage of tunneling from GaAs is that the polarization of the photo-excited electrons can be easily reversed by reversing the helicity of the light from left to right circular polarization. The photo-excited electrons are polarized along the axis defined by the direction of the light which is also the axis of the light angular momentium. The optical selection rules for circularly polarized light produce a polarization of photo-excited electrons of 50%. Spin relaxation can reduce this; for example, the spin polarization of photo-emitted electrons ranges from 25% to 50%. The magnetic field from the surface under investigation may add a further depolarization mechanism. The precession of optically excited electrons in the magnetic field, known as the Hanle effect, has been measured for GaAs by spin-polarized luminescence. A decrease of the polarization by as little as a factor of two in a field as high as 10 kOe has been reported [27, 28].

Two configurations have been contemplated: (1) the incident light is along the tip axis producing a tunneling spin polarization suitable for investigating spin configurations aligned perpendicular to the sample surface, and (2) the incident light is transverse to the tip axis suitable for investigating spin configurations parallel to the sample surface. In the second configuration, the high index of refraction of GaAs ($n = 3.4$) causes the light inside the tip to travel nearly normal to the surface of the side of the tip leading to deviations from pure transverse spin polarization. Further problems such as the effect of scattered light and the behavior of these small structures as optical waveguides must also be considered.

A crucial question is whether a sufficient number of electrons can be excited to the conduction band for observable tunneling. Tunneling from dopant levels in *p*-type GaAs at a density of $10^{18}\,\mathrm{cm}^{-3}$ has been observed by Feenstra and Stroscio to produce currents about four orders of magnitude less than the electron tunneling out of the valence band or into the conduction band [29]. Taking this as an approximate limit of detectability, we calculate the light power required to achieve an excited state electron density of $10^{18}\,\mathrm{cm}^{-3}$. For a photon energy of 1.5 eV, there are 4×10^{15} photons $\mathrm{s}^{-1}\,\mathrm{mW}^{-1}$. If it is assumed that the light is focused in a 10 μm diameter spot and is absorbed to $1/e$ of its intensity in 1 μm, the excitation rate of electrons into the conduction band is $2 \times 10^{25}\,\mathrm{el\,cm}^{-3}\,\mathrm{s}^{-1}\,\mathrm{mW}^{-1}$. The photo-excited electrons recombine readily with holes and have a lifetime of about 10^{-9} s for $10^{18}\,\mathrm{cm}^{-3}$ *p*-type doping. (We consider *p*-type material as the favorable case since band bending in *n*-type material increases the tunneling barrier and provides a reservoir of electrons which dilutes the polarization of the conduction-band electrons). This calculation leads to a steady-state excited-electron density of $2 \times 10^{16}\,\mathrm{el\,cm}^{-3}\,\mathrm{mW}^{-1}$. With 50 mW of light focused into a 10 μm diameter spot, the required excited-electron density should be achieved.

Illuminating splinters of GaAs in air with a light intensity of 300 mW and wavelength of 589 nm for 5 min produced tip damage in the form of melting that was clearly observable in an optical microscope [30]. Even if a tip does not actually melt, the heating of the tip and sample leads to very poor positional stability in the STM.

In order to make polarized tunneling from an optically pumped semiconductor feasible, it is desirable to be able to work with lower light intensities. A longer electron lifetime increases the photo-excited carrier density for a given light intensity. A factor of two or so longer lifetime is about all that can be gained even in GaAs with an especially low defect concentration. However, since a negative-electron affinity is not required for tunneling, as it is in the case for photo-emission of polarized electrons, other semiconductors can be considered. Other semiconductors with spin-orbit split bands may have better properties than GaAs with regard to longer excited-electron lifetime, resistance to thermal damage, and role of surface states and surface recombination (which will not be discussed here but which add further complications).

It may also be possible to work with smaller tunneling currents than we have used in our estimates. In the spectroscopic mode, the tip position is set by tunneling from the filled sample states into the GaAs conduction band (or from the GaAs valence band into empty sample states) and held at that position while the bias is changed to measure the small tunneling current of optically excited electrons, as shown schematically in Fig. 5. In the $10^{18}\,\mathrm{cm}^{-3}$ *p*-type GaAs we have been using as an example, the bands would bend down at the surface. However, the densities of photo-excited carriers we are considering would have the effect of flattening the bands when illuminated, an effect which can be accounted for in the spectroscopic measurement mode proposed.

6. Conclusions

The use of the inherent spatial resolution of the scanning electron microscope combined with secondary-electron polarization analysis (SEMPA) has proven an excellent way to investigate spin structures such as magnetic domains. For the alternative SEM technique wherein a low-energy spin-polarized electron beam is used in the SEM, several important limitations were discussed.

The scanning field-emission analog to SEMPA may afford higher resolution when specially made single-atom tips are used. While a great many unanswered questions remain, there appears to be the possibility of imaging spin configurations with < 30 Å lateral resolution.

Finally, the tunneling of polarized electrons from ferromagnetic tips or from an optically pumped semiconductor tip offers the tantalizing possibility of atomic-resolution images of spin configurations. The great advantages afforded by the ability to easily reverse the electron spin polarization in tunneling from GaAs, in order to detect small spin-dependent

signals, makes it worthwhile to think about ways to get around the difficulties we have discussed.

There have been great advances in STM instruments and measurement techniques in just a few years. There is reason to believe that the requisite measurement sensitivity may be obtained to allow lower light intensity and that other problems could be overcome which would make feasible the proposed measurement utilizing spin dependent tunneling from an optically-pumped semiconductor tip.

Acknowledgements

Stimulating discussions with many NBS colleagues, particularly R. J. Celotta, S. M. Girvin, J. J. McClelland, and D. R. Penn are gratefully acknowledged. This work was supported in part by the Office of Naval Research.

References

1. Bitter, F., Phys. Rev. **38**, 1903 (1931).
2. Newbury, D. E., Joy, D. E., Echlin, P., Fiori, C. E. and Goldstein, J. I., Advanced Scanning Electron Microscopy and X-ray Microanalysis, Plenum Press, New York (1986).
3. Jakubovics, J. P., Electron Microscopy in Materials Science Part IV (Edited by E. Ruedl and U. Valdre), p. 1305, Commission of European Communities, Brussels (1973).
4. Kranz, J. and Hubert, A., Z. Angew. Phys. **15**, 220 (1963).
5. Hembree, G. G., Unguris, J., Celotta, R. J. and Pierce, D. T., Physical Aspects of Microscopic Characterization of Materials (Edited by J. Kirschner *et al.*), Scanning Microscopy, Suppl. 1, 229 (1987).
6. Koike, K., Matsuyama, H. and Hayakawa, K., Physical Aspects of Microscopic Characterization of Materials (Edited by J. Kirschner *et al.*), Scanning Microscopy, Suppl. 1, 241 (1987).
7. Unguris, J., Pierce, D. T., Galejs, A. and Celotta, R. J., Phys. Rev. Lett. **49**, 72 (1982).
8. Kessler, J., Polarized Electrons, Spinger, New York (1976).
9. Unguris, J., Pierce, D. T. and Celotta, R. J., Rev. Sci. Instrum. **57**, 1314 (1986).
10. Koike, K. and Hayakawa, K., Jpn. J. Appl. Phys. **23**, L187 (1984).
11. Celotta, R. J. and Pierce, D. T., Microbeam Analysis-1982 (Edited by K. F. J. Heinrich), p. 469, San Fransisco Press (1982).
12. Kirschner, J., Scanning Electron Microsc. 1984, III: 1179 (1984).
13. Celotta, R. J., Pierce, D. T., Wang, G. -C. Bader, S. D. and Felcher, G. P., Phys. Ref. Lett. **43**, 728 (1979).
14. Siegmann, H. C., Pierce, D. T. and Celotta, R. J., Phys. Rev. Lett. **46**, 452 (1980).
15. Pierce, D. T., Celotta, R. J., Wang, G. -C. Unertl, W. N., Galejs, A., Kuyatt, C. E. and Mielczarek, S. R., Rev. Sci. Instrum. **51**, 478 (1980).
16. Kisker, E., Baum, G., Mahan, A. H., Raith, W. and Reihl, B., Phys. Rev. **B18**, 2256 (1978).
17. Pierce, D. T., Celotta, R. J., Siegmann, H. C. and Unguris, J., Phys. Rev. **B26**, 2566 (1982).
18. Binnig, G. and Rohrer, H., IBM J. Res. Develop. **30**, 355 (1986).
19. Young, R., Ward, J. and Scire, F., Rev. Sci. Instrum. **43**, 999 (1972).
20. Reihl, B. and Gimzewski, J. K., Surf. Sci. **189/190**, 36 (1987).
21. Fink, H. W., IBM J. Res. Develop. **30**, 460 (1986).
22. Fink, H. W., Proc. Adriatico Research Conference on "Scanning Tunneling Microscopy – Fundamental Experimental and Theoretical Progress", July 28–31, 1987. Physica Scripta (to be published) and private communication.
23. Landolt, M. and Yafet, Y., Phy. Rev. Lett. **40**, 1401 (1978).
24. Gadzuk, J. W., Phys. Rev. **182**, 416 (1969).
25. Maekawa, S. and Gäfvert, U., IEEE Trans. on Magnetics **MAG-18**, 707 (1982).
26. Gao, Y. and Reifenberger, R., Phys. Rev. **B32**, 1380 (1985).
27. Garbuzov, D. Z., Ekimov, A. E. and Safarov, V. I., JETP Lett. **13**, 24 (1971).
28. Fishman, G. and Lampel, G., Phys. Rev. **B16**, 820 (1977).
29. Feenstra, R. M. and Stroscio, J. A., J. Vac. Sci. Technol. **B5**, 923 (1987).
30. McClelland, J. J., Private Communication.